A synchrotron X-ray scattering study of the crystallization behavior of mixtures of confectionary triacylglycerides: effect of chemical composition and shear on polymorphism

Food Research International 177 (2024) 113864

Contents lists available at ScienceDirect

Food Research International

journal homepage: www.elsevier.com/locate/foodres

A synchrotron X-ray scattering study of the crystallization behavior of mixtures of confectionary triacylglycerides: Effect of chemical composition and shear on polymorphism and kinetics

Elena Simone [a,b,*], Michael Rappolt [b], Holly Ewens [b], Tom Rutherford [c], Stephanie Marty Terrade [d], Francesca Giuffrida [d], Cynthia Marmet [d]

[a] Department of Applied Science and Technology (DISAT), Politecnico di Torino, Torino, Italy
[b] School of Food Science and Nutrition, Food Colloids and Bioprocessing Group, University of Leeds, Leeds, United Kingdom
[c] Nestlé Product Technology Centre Confectionery, Haxby Road, York, YO31 8TA, United Kingdom
[d] Nestlé Research, Vers-chez-les-Blanc, Lausanne 26, 1000, Switzerland

ARTICLE INFO

Keywords:
Cocoa butter
Crystallization
X-ray scattering
Triacylglycerides (TAGs)

ABSTRACT

Cocoa butter equivalents (CBE) are mixtures of triglycerides from multiple sources (e.g., sunflower oil, mango kernel and sal), which resemble cocoa butter (CB) in both physical and chemical properties. Despite being widely used to replace CB in chocolate products, the crystallization behavior of many CBEs is still poorly understood. The aim of this work was to develop a fundamental understanding, at the molecular level, of the crystallization behavior of selected CBEs, and compare it with that of CB. Chromatography was used to determine the composition of CBEs, in terms of fatty acids and triacylglycerides (TAGs), while their thermodynamic behavior and crystallization kinetics were studied using polarized microscopy, differential calorimetry and three different synchrotron X-ray scattering setups. CBEs of different origin and chemical composition (e.g., different ratios of the main CB TAGs, namely POP, SOS and POS) crystallized in different polymorphs and with different kinetics of nucleation, growth and polymorphic transformation. SOS rich CBEs presented showed more polymorphs than CB and POP rich samples; whereas, CBEs with high concentration of POP showed slow kinetic of polymorphic transformation towards the stable β(3L) form.

Additionally, it was observed that the presence of small amounts (<1% w/w) of specific TAGs, such as OOO, PPP or SSS, could significantly affect the crystallization behavior of CBEs and CBs in terms of kinetics of polymorphic transformation and number of phases detected (multiple high melting β(2L) polymorphs were identified in all samples studied). Finally, it was found that, regardless of the CBE composition, the presence of shear could promote the formation of stable β polymorphs over metastable β' and γ forms, and reduced the size of the crystal agglomerates formed due to increased secondary nucleation.

1. Introduction

Chocolate is a popular food product, whose demand has been constantly increasing over the past years (Ewens et al., 2021; Metilli et al., 2021). However, the current production of cocoa is not able to fully meet such demand, causing an increase in the market price of this commodity (Norazlina et al., 2021). For this reason, chocolate manufacturers have started to develop strategies to replace or reduce the amount of cocoa used in chocolate (Ewens et al., 2021). One of them is the use of cocoa butter equivalents (CBE), which are mixtures of triacylglycerols (TAGs) from multiple sources (e.g., sunflower oil, mango kernel and sal) that resemble cocoa butter (CB), in both physical (e.g., melting range and crystal morphology) and chemical properties (e.g., fatty acids and TAGs profiles) (Ghazani & Marangoni, 2019).

A good CBE should present the same functional properties of CB in chocolate products (Bahari & Akoh, 2018; Castro-Alayo et al., 2023; Hadri et al., 2022; Lipp et al., 2001); in order to achieve this goal different fractions of fats from different sources can be blended to form a CBE (Norazlina et al., 2021). As an alternative route chemical modifications, such as enzymatic esterification, can be applied to fats or oils (e.

* Corresponding author.
E-mail address: elena.simone@polito.it (E. Simone).

https://doi.org/10.1016/j.foodres.2023.113864
Received 25 September 2023; Received in revised form 8 December 2023; Accepted 14 December 2023
Available online 21 December 2023

g., sunflower and safflower oils) (Bahari & Akoh, 2018; Ghazani & Marangoni, 2019; Sivakanthan & Madhujith, 2020) to obtain the desired melting range and TAGs composition.

Nevertheless, it is not possible to achieve the exact same TAGs composition of CB by mixing blends of other fats or via interesterification. This is an issue, when it comes to precisely controlling chocolate crystallization. Minimal differences in TAGs composition, even those among CBs harvested in different regions, might lead to different kinetics of nucleation and growth as well as different structure and morphology of fat crystals (Bouzidi & Narine, 2012; Ghazani & Marangoni, 2019, 2021; Marty-Terrade & Marangoni, 2012; Sasaki et al., 2012; Sato & Ueno, 2005).

CB normally contains in weight about 26 % palmitic acid, 36 % stearic acid, 34 % oleic acid, 2.7 % linoleic, and 0.9 % arachidic acid (Metilli et al., 2021). These fatty acid mostly form disaturated 1,3-distearoyl-2-oleoyl glycerol (SOS), 1(3)-stearoyl-2-oleoyl-3(1)-palmitoyl glycerol (POS) and 1,3-dipalmitoyl-2-oleoyl glycerol (POP) with oleic acid in the *sn*-2 position of glycerol backbone. TAGs crystallize in three main crystal structures. In order of thermodynamic stability these are: (1) the α polymorph, with a hexagonal 3D-subcell of chain packing, (2) the β' polymorph with an orthorhombic-perpendicular 3D-subcell of chain packing and (3) the β polymorph with a 3D-triclinic parallel subcell of chain packing (Abrahamsson et al., 1978) (it is worth noting that the corresponding 2D-subcells of chain packing are hexagonal, rectangular and oblique (Small, 1984)). Furthermore, TAGs polymorphs differ in the way their fatty acid chains are stacked. Two very common stacking repeats are observed, being two (2L) or three (3L) fatty acid chain lengths long (Ladd Parada et al., 2018; Pratama et al., 2022; Timms, 1984). Some TAGs or TAGs mixtures can also crystallize in the metastable γ polymorph, which has similar structure to the β'(3L) polymorph (Lipp et al., 2001; Mykhaylyk & Hamley, 2004). Depending on the mixture of TAGs that form a specific fat, different types and combinations of stacking and chain packing can exist. CB can crystallize in six different structures, with the β polymorph of form V being the ideal polymorph to give chocolate a glossy appearance, the correct melting point and a good snap. Despite its widespread use, the mechanisms of nucleation and polymorphic transformation from one CB crystal structure to another are still poorly understood and subject of ongoing debate (Bresson et al., 2021; Ghazani & Marangoni, 2023; Ladd-Parada et al., 2019; Marty-Terrade & Marangoni, 2012; Pirouzian et al., 2020; Toro-Vazquez et al., 2012). Even less is known about the crystallization behavior of cocoa butter equivalents (CBEs) and how they affect chocolate crystallization when mixed with CB (Bahari & Akoh, 2018; Castro-Alayo et al., 2023).

In this work synchrotron X-ray scattering, differential scanning calorimetry (DSC), rheological measurements and polarized light microscopy were used, providing a comprehensive overview of the crystallization behavior of very different CBEs and CBs, with accurate structural information of the possible phases that can form from specific TAGs mixtures and considering also the effect of shear (e.g., rheometer experiments) on the kinetics of nucleation, growth and polymorphic transformation of such phases. The experimental results were interpreted in light of the TAGs and fatty acids composition of each sample analyzed. In this work we did not just focus on the effect of different ratios of the three main CB TAGs (SOS, POP, POS), but we investigated the effect of TAGs contained in minor amounts (e.g., tri-saturated, di-unsaturated and tri-unsaturated) on the polymorphic landscape of CBEs and on the kinetics of crystallization.

Using this approach allowed gaining a molecular-level understanding of the crystallization process for the analyzed edible fats, and identifying multiple highly stable phases that has not been observed previously in this type of samples. Such fundamental knowledge is essential for the rational design of novel chocolate recipes that uses CBEs, but also for the understanding of the crystallization behavior of other edible mixtures of TAGs that might be used in food, cosmetic or pharmaceutical applications (Metilli et al., 2022; Ramos-de-la-Peña et al., 2021).

2. Materials and methods

2.1. Materials

Samples of cocoa butter and cocoa butter equivalents were kindly provided by the Nestlé Product Technology Centre Confectionery in York (UK). The company provided a series of ingredients from several manufacturers and geographical origin that were used for different purposes in their confectionary formulations. CB and S6 were both cocoa butter samples of different origin, Ghanian and Brazilian, respectively. Samples S1 to S5 and S7 to S14 were cocoa butter equivalents of different origin, including mixtures of palm, shea and sal fats, as well as interesterified sunflower and safflower oils.

2.2. Chemical characterization

Samples were characterized chemically in terms of fatty acids (FA) and triacylglycerides composition by chromatography. An Accela 1250 liquid chromatograph (Thermo Fisher Scientific, Bremen, Germany) equipped with a Agilent Poroshell 120 EC-C18 (2.7 μm particle size, 2.1 × 250 mm) was used for separation of analytes; while an LTQ-Orbitrap XL hybrid mass spectrometer (Thermo Fisher Scientific, Bremen, Germany) was used for the identification of the TAGs and FAs that characterized each sample. The detailed experimental procedure is described elsewhere (Nagy et al., 2013).

2.3. Differential scanning calorimetry (DSC)

The DSC curves were obtained using a PerkinElmer calorimeter (DSC 8000, PerkinElmer Corp., Waltham, USA), combined with a cooling system (Intracooler 2, PerkinElmer, USA). The purge gas used was nitrogen (99.99 % purity) at a flow rate of 20 mL/min. Sample preparation consisted of placing 1.35 ± 0.001 mg of molten fat in aluminium pans (30 μL - Part No. BO14-3016, PerkinElmer, Germany). The pans were then covered with aluminium lids (Part No. BO14-3003, PerkinElmer, Germany) and hermetically sealed. As a reference, an empty sealed aluminium pan was measured. The results were analyzed using the software Pyris DSC 8000. To avoid differences in crystallization behavior related to secondary nucleation phenomena or differences in the thermal history, all samples were fully molten at 70 °C before characterization with all techniques presented in this paper. For DSC, the thermal protocol applied for each sample was the following: (i) Melting and holding for 10 min at 70 °C, (ii) cooling to 18 or 20 °C at a rate of around −70 °C/min and holding for 120 min at this temperature, (iii) heating the sample up to 25 °C and holding for 15 min, and finally, (iv) cooling the sample down to 15 °C and holding it for 30 min at this temperature. At the end of each thermal protocol, samples were cooled to −30 °C at a rate of around −40 °C/min to induce the solidification of the lower melting TAGs and then heated up again to 70 °C. It is worth noting that this final step minimizes the occurrence of polymorphic transformations during the heating stage, allowing a more precise identification of the solid phases formed during the isothermal hold.

2.4. Polarized light microscopy (PLM)

Selected samples (S1, S2, CB, S10 and S13) were analyzed with PLM. Samples were heated to 65 °C until fully molten. Then 50 μL of sample was pipetted onto a Linkam CSS450 hot plate connected to a liquid nitrogen pump (Linkam Scientific Instruments, UK). The hot plate was closed and a gap of 100 μm was set. The hot plate was controlled with the Linksys32 control software (Linkam Scientific Instruments, 2003) and placed under a Leitz Dialux 22 microscope with a polarized light lens (Leica Microsystems, Germany). The sample was heated to 70 °C and kept there for 10 mins. Then the sample was cooled to 45 °C at

−30 °C/min and held there for 3 mins. Liquid nitrogen was used to cool the sample. The temperature was then decreased to 20 °C at a rate of −1°C/min and held there for 2 h. At the start of this cooling stage, a Canon EOS 7D Mark II camera (Canon, Japan) was controlled using the software digiCamControl (Istvan, 2020), taking pictures every 1 min through a 40x lens (Nikon, Japan). After the 2 h, the sample was heated back to 45 °C at a rate of 1 °C/min. The shearing experiments were conducted using the same temperature profile; the experiments were stopped, when the sample was fully solid at 20 °C. The three shear speeds used were 0.25 rad/s, 0.15 rad/s and 0.05 rad/s.

2.5. Synchrotron small angle X-ray scattering – Multi-capillary holder

The polymorphs arising from crystallization of each sample were determined using synchrotron radiation X-ray diffraction (SR-XRD, λ = 0.69 Å) at the beamline I22 at the Diamond Light Source (DLS, Didcot, U.K.). The sample-to-detector distance (SDD) was set to 4.716 m for the SAXS, and the 2D diffraction patterns were recorded on a Pilatus 2 M detector (Dectris Ltd., Switzerland). For WAXS a Pilatus P3-2 M−DLS−L (silicon hybrid pixel detector, Dectris Ltd., Switzerland) was used, positioned at 163.5 mm from the sample. Disposable polycarbonate capillaries (diameter 2 mm) were filled with mixtures of melted samples and loaded into a temperature-controlled multi-capillary rack, connected to an external water bath (Lauda, Germany). The temperature was initially set to 70 °C for 10 min, and then cooled down to 20 °C at a rate of −1 °C/min. The temperature was then kept constant for 2 h and then raised to 25 °C for 15 min to remove the more metastable phases. After this step, each sample was cooled down to 20 °C and kept at this temperature for up to 4–5 h. The exposure time was set to 1.0 s. An empty polycarbonate capillary was used for background scattering subtraction. Diffraction images were processed using the software DAWN (Filik et al., 2017). The resulting 1D data were extracted, sorted and analyzed using MATLAB 2021a, Excel 2020 and Origin Pro 2020 (peak fitting function). Both SAXS and WAXS plots were used to identify the number and type of phases present in the samples. Hereby, WAXS data are more informative at higher values of solid fat content (e.g., after long term storage at ambient temperature); whereas, in the early stages of crystallization, due to the strong scattering contribution of the liquid phase, it is more challenging to identity the different polymorphs from this q region.

First, to obtain the trends for the peak intensities over time, the second derivative of SAXS curves were calculated, in order to separate overlapping peaks. These second derivative curves were then multiplied by −1, obtaining positive second derivative peaks at the same position as that of the corresponding Bragg peaks. The height of such peak was then plotted to monitor the evolution of the crystallization of the given polymorph (Ollivon et al., 2006). Second, the second derivative trends were normalized to the actual intensity of the corresponding Bragg peak (Gaussian and Voigt distributions applied). Note, Gaussian-shaped peaks are appropriate for fitting the β-phases, which display thermal disorder, while all other phases are displaying only quasi-long range order and are most appropriately fitted with Voigt distributions (Rappolt, M.; Laggner, P.; Pabst, 2004).

2.6. Benchtop small angle X-ray scattering

This technique was used to analyze the kinetics of polymorphic transformations over a long period of time (up to six months). Measurements were carried out with a SAXSpace instrument (Anton Paar GmbH, Graz, Austria) equipped with a Cu anode (λ = 1.54 Å) and operating at 40 kV and 50 mA. The sample holder is equipped with a Peltier element (TCstage 150, Anton Paar GmbH, Graz, Austria), which provides temperature control in a range of −30 to +150 °C (±0.1 °C). Simultaneous SAXS/WAXS measurements were performed at a sample–detector distance of 130 mm, which covers a q range from 0.01 to 1.76 $Å^{-1}$ ($q = 4\pi(\sin\theta)/\lambda$, with 2θ being the scattering angle). The 1D scattering patterns were recorded with a Mythen microstrip X-ray detector (Dectris Ltd., Baden, Switzerland). The position of the primary beam of all diffraction patterns was set to zero, using the SAXSTreat software (Anton Paar GmbH, Graz, Austria). The SAXSQuant software (Anton Paar GmbH, Graz, Austria), was used to normalize all recorded scattering patterns for their sample transmission, i.e., divided by their measured transmitted direct beam intensity. From each normalized sample pattern the normalized empty capillary scattering was then subtracted. Samples were subjected to the same temperature profile described in the previous section.

2.7. Synchrotron small angle X-ray scattering – Simultaneous DSC and SAXS

The in-line DSC (Ollivon et al., 2006) available at the Austrian SAXS beamline at the Elettra Sincrotrone Trieste (Italy) was used for simultaneous DSC and SAXS/WAXS measurements. A Pilatus3 1 M detector (Dectris, DH) at a SDD of 1.3 m was used for the SAXS signal (range = $0.76 < q < 57.5$ $Å^{-1}$), while a Pilatus 100 k detector was used for the WAXS region (range = $63 < q < 163$ $Å^{-1}$). The energy of the beam was 8 keV (1.54 Å wavelength) and the calibration was performed with silver behenate (d-spacing 58.38 Å) for the SAXS and p-bromobenzoic acid for the WAXS region. The sample holder was a quartz capillary of 1.4 ± 0.1 mm of diameter and about 80 mm length, which was inserted into the in-line DSC; an empty capillary of the same size was used as reference to estimate the thermal signal. Capillaries were filled with molten samples at 50 °C. After positioning the samples in the DSC setup, the temperature was raised to 70 °C and then samples were cooled down to 20 °C at −1°C/min and kept at this temperature for 2 h. Then the temperature was raised to 25 °C at a rate of 1 °C/min, kept for 15 min and then brought back to 20 °C for at least another hour. The same capillaries used for DSC-SAXS experiments were stored at ambient conditions for 6 months and then measured at the same beamline to check the effect of long term storage.

The 2D images were processed using the SAXSDOG software (Burian et al., 2022). Processed data were further analyzed using MATLAB 2021a, Excel 2020 and Origin Pro 2020.

2.8. Synchrotron small angle X-ray scattering – Rheometer

The final set of SAXS experiments was performed on the beamline ID02 at the European Synchrotron (ESRF) located in Grenoble (France), using the stress controlled rheometer setup (a commercial Thermo-Haake RS6000) equipped with an X-ray transparent Couette cell. The concentric cylinders of the cell used (inner diameter 20 mm, outer diameter 22 mm, and height 40 mm) were machined out of Vespel polymer. An Eiger2 4 M detector (Dectris, DH) was used for the SAXS signal (range = $0.45 < q < 58.4$ $Å^{-1}$), while a Rayonix LX 170HS (Rayonix, US) detector was used for the WAXS (range = $56.8 < q < 351.7$ $Å^{-1}$). The energy of the beam was 12.5 keV (1 Å wavelength). The CBE and CB samples were molten at 50 °C in an oven and then around 2 mL of sample was transferred into the Couette cell using a plastic pipette. The temperature was raised to 70 °C and then cooled down to 23 °C at a cooling rate of −2 °C/min. Since the available temperature controller was not very effective in maintaining a temperature below 26 °C compressed air was flown towards the Couette cell after being cooled in a coaxial heat exchanger, using cold water as refrigerant (a photo of the modified setup is shown in Supporting Information, Fig. S1). The temperature profile was applied in the absence of shear and applying a shear of 1000 s^{-1}. Raw X-ray data were processed using the custom written software PyFAI, following a procedure described in detail elsewhere (Narayanan et al., 2018). Processed X-ray and viscosity data (collected by the equipment software) were further extracted and analyzed using MATLAB 2021a, Excel 2020 and Origin Pro 2020.

Table 1
Fatty acid composition for all the analyzed samples.

Fatty acid	S1	S2	S3	S4	S5	S6	S7	S8	S9	S10	S11	S12	S13	S14	CB
Palmitic	6.5	25.6	31.7	28.6	5.7	26.1	33.9	37	30.1	47.4	34	35.3	31.8	36	25.2
Oleic	40.6	32.9	31.7	33	41.1	32	32.4	31.8	32.6	31.6	30.9	30.6	32.1	30.9	31.4
Stearic	43.8	29.9	27.8	30.1	44.5	33.5	25.3	21.9	26.1	10.9	25.9	25.3	27.4	24.2	34.9
Other	4.7	6.9	4.2	3.7	4.3	3.8	3.7	4.6	6.4	5.4	4.7	4.4	3.7	4.3	3.6
Saturated (%)	51.7	60.4	60.8	59.7	51.7	60.6	60.2	60.1	60.5	59.6	61.4	62.1	60.3	61.5	61
Unsaturated (%)	43.9	34.9	34.6	35.7	43.9	34.8	35.1	35.2	34.7	35.7	34.1	33.5	34.7	33.9	34.1
Average FA chain length (number of C)	17.9	17.6	17.4	17.4	17.9	17.5	17.3	17.2	17.5	17.0	17.3	17.3	17.3	17.3	17.5

Table 2
Triacylglyceride (TAG) composition of each sample.

TAG type	S1	S2	S3	S4	S5	S6	S7	S8	S9	S10	S11	S12	S13	S14	CB
POP	2.4	28.2	35.3	31.3	1.8	18.2	41.3	40.3	34.5	49.4	37.3	40.2	35.2	39	16.9
SOS	41.2	31.3	29.9	34.1	42.9	25	28.5	23.8	26.6	7.8	27.3	28.6	29.6	23.8	27
POS	10.5	12.3	11.4	11	9.3	37	10	10.4	12.1	11.1	11.1	10.6	14.6	13.8	37.3
Tri-saturated	1.5	<1	1.4	<1	1.6	<1	1	1.5	<1	3	1.6	1.6	<1	1.5	<1
Tri- and di-unsaturated	36.1	8.2	11.1	12.1	35.6	12.7	9.8	11.6	8.5	14.7	12.5	9.7	10.1	11.2	11.8
Other monosaturated	1.3	9.7	3.4	1.5	1.1	1.4	2.5	4.3	8	3.7	3.5	2.7	1.6	3.9	1.3

P stands for palmitic, O for oleic and S for stearic acid. Tri-saturated TAGs include SSS and PPP. Tri and di-unsaturated TAGs include OOS, OOP, OOO together with TAGs containing linoleic acid (18:2). Other mono-saturated TAGs include ones containing oleic acid and other saturated FAs with chain length ranging from 14 to 22C atoms.

2.9. Electron density profiles (EDPs)

EDPs were calculated using a standard Fourier transform procedure (Pratama et al., 2022). The Braggs peak intensity were obtained from the fitted area and were Lorentz corrected, meaning that the intensity $I(h)$ was multiplied by h^2, where h is the Miller index (diffraction order). Then, the amplitude values F_h were obtained from the square root of the corrected intensity. For centrosymmetric EDPs, the Fourier transform is obtained by Eq. (1):

$$\Delta\rho(z) = \sum_{h=1}^{h_{max}} \alpha_h F_h cos\left(\frac{2\pi z h}{d}\right) \quad (1)$$

where $\Delta\rho(z)$ is the electron density contrast, α_h denotes the phases (for h = 1, α_h was set to −1, which places the bilayer core at $x = 0$ nm) and d denotes the lattice spacing. The phases α_h for values of h from 2 to 6 were taken from the literature (Mykhaylyk & Hamley, 2004).

3. Results and discussion

3.1. Chemical composition of CB and CBEs

Table 1 shows the FA composition for each sample. Despite similar origin the composition of the different samples present many differences, particularly in the concentration of minor TAGs, such as tri-saturated or di-unsaturated ones. For all samples the main FAs are the ones typical of cocoa butter: stearic, palmitic and oleic. CB and S6 present similar content of these three FAs, with slightly higher content of stearic and oleic rather than palmitic. Sample S10 presents the highest content of palmitic acid (47.4 %) and lowest of stearic (10.9 %) among all samples; whereas S1 and S5 are very similar and have the highest content of stearic acid (43.8 and 44.5 %) and lowest of palmitic (<7%) of all samples. The high amounts of palmitic acid in S10 and of stearic acid in S1 and S5 explains why they have respectively the lowest and highest average chain length (17.0 versus 17.9 C atoms).

Samples S1 and S5 are characterized by a higher amount of unsaturated fatty acids compared to the rest of the samples: over 43.9 % compared to 34–36 % of the other samples. The percentages of saturated and unsaturated fatty acid, as well as the average FA chain length, are very similar to that of cocoa butter (CB and S6) for samples S2 to S4 and S7 to S14, despite their different origin. Finally, the two cocoa butter samples are characterized by a lower amount of palmitic acid compared to the aforementioned CBEs.

Table 2 shows the TAGs composition of each sample analyzed. It is evident that the highest content of POS is given in the two cocoa butter samples CB and S6 when compared to the CBEs. Sample S10 has the highest content of POP compared to the other samples, while S1 and S5 have the highest concentration of SOS. Furthermore, these two samples have the highest content of di- and tri-unsaturated TAGs. It is worth also noticing the high amount of tri-saturated TAGs in S10 (almost two-fold), when compared to all the other samples. In the following sections the effect of the different chemical composition of each sample is examined.

3.2. Polymorphism of CB and CBEs during cooling crystallization

Despite small differences in the chemical composition, synchrotron X-ray experiments in capillaries (stagnant conditions) showed very different crystallization behavior for the analyzed samples. All phases detected for each sample and their corresponding d-spacings are summarized in Table 3. The two cocoa butter samples CB and S6 showed similar behavior, with the α polymorph (2L stacking) nucleating first and then transforming into the β'(2L) and finally the β(V) polymorph.

Table 3
D-spacings in å for all polymorphs detected in each sample. N.d. = not detected. *=sample after long storage was not measured at synchrotron.

Polymorph	S1	S2	S3	S4	S5	S6	S7	S8	S9	S10	S11	S12	S13	S14	CB
α(2L)	51	50	49	50	51	49		49	50	48	49	49	50	49	49
β'(2L)	45	45	44	44	45	44	44	44	45	42	45	45	45	44	44
β'(3L)	80	n.d.	n.d.	n.d.	78	n.d.	n.d.	n.d.	n.d.	n.d.	n.d.	n.d.	n.d.	n.d.	n.d.
γ(3L)	71	n.d.	n.d.	n.d.	70	n.d.	n.d.	n.d.	n.d.	n.d.	n.d.	n.d.	n.d.	n.d.	n.d.
β(3L)	65	66	63	64	65	64	64	65	66	65	64	64	65	65	64
β(2L)	45, 50	43, 48	43, *	43, *	*	43, 44, 50	43, 48	43, *	43, *	n.d.	43, *	43, *	43, 49	43, *	43, 44, 50

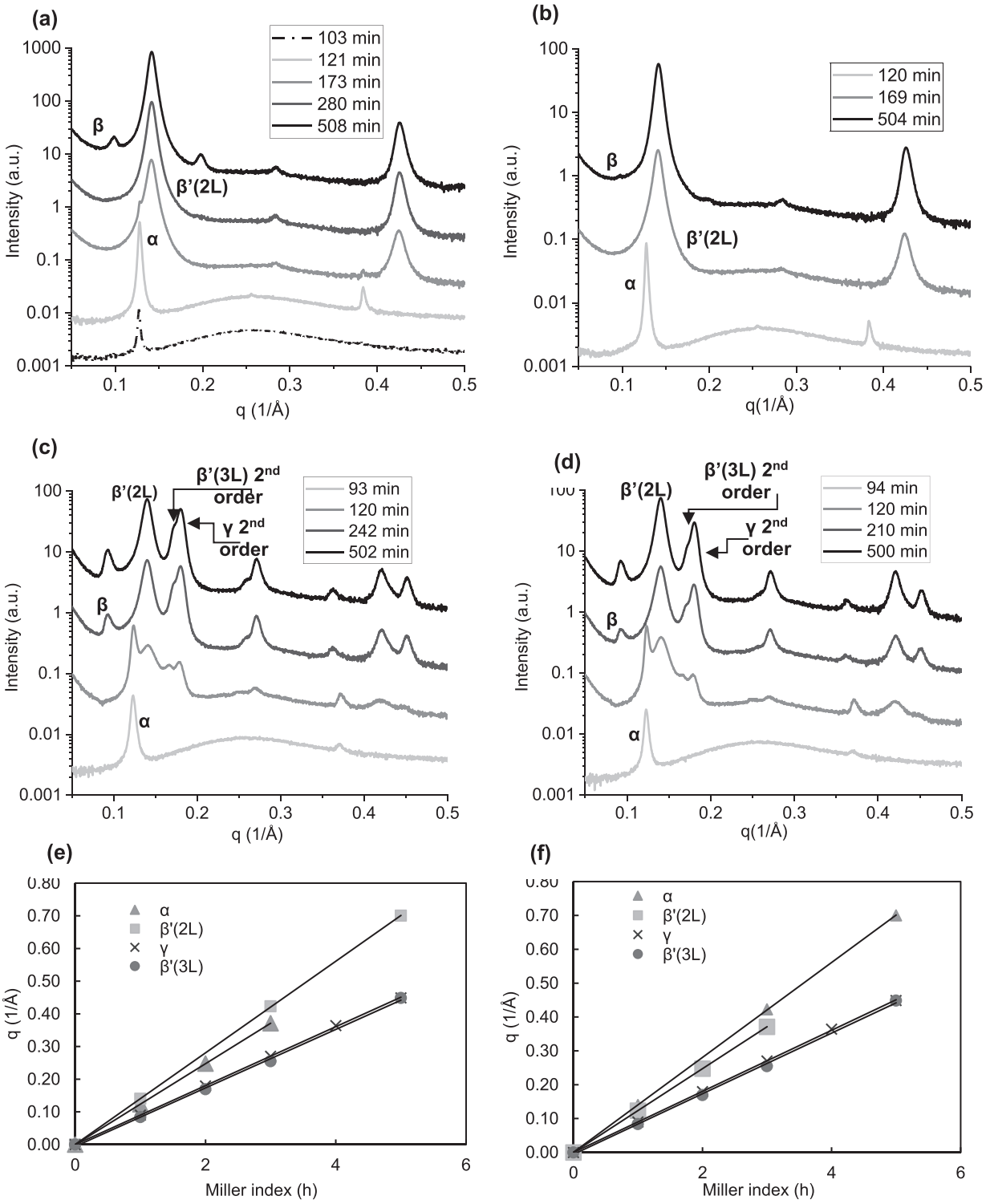

Fig. 1. SAXS pattern the CB and handpicked CBE samples. The SAXS pattern of CB (a), S6 (b), S1 (c) and S5 (d) during isothermal crystallization experiments in the multi-capillary holder are presented. The indexing of sample S1 and S5 are shown in panel (d) and (e), respectively. The time = 0 is set at the start of the cooling profile.

The d-spacings of all polymorphs of CB and S6 were identical: 49 Å for the α, 44 Å for the β'(2L) and 64 Å for the β(V) structure. It is worth noticing, that the transformation from the β'(2L) to the β(V) polymorph was faster for CB than for S6 (Fig. 1a and b); in fact, only traces of the most stable form are visible in sample S6 at 500 min from the start of the cooling profile. This difference in the kinetics of polymorphic transformation might be due to the presence of a higher amount of tri-unsaturated OOO in the CB sample compared to S6 (1.8 % and <1 %). The effect of tri-unsaturated TAGs on the kinetics of polymorphic transformation was observed previously in the literature (Campos et al., 2010). In both samples the α-forms rapidly disappear before the heating to 25 °C.

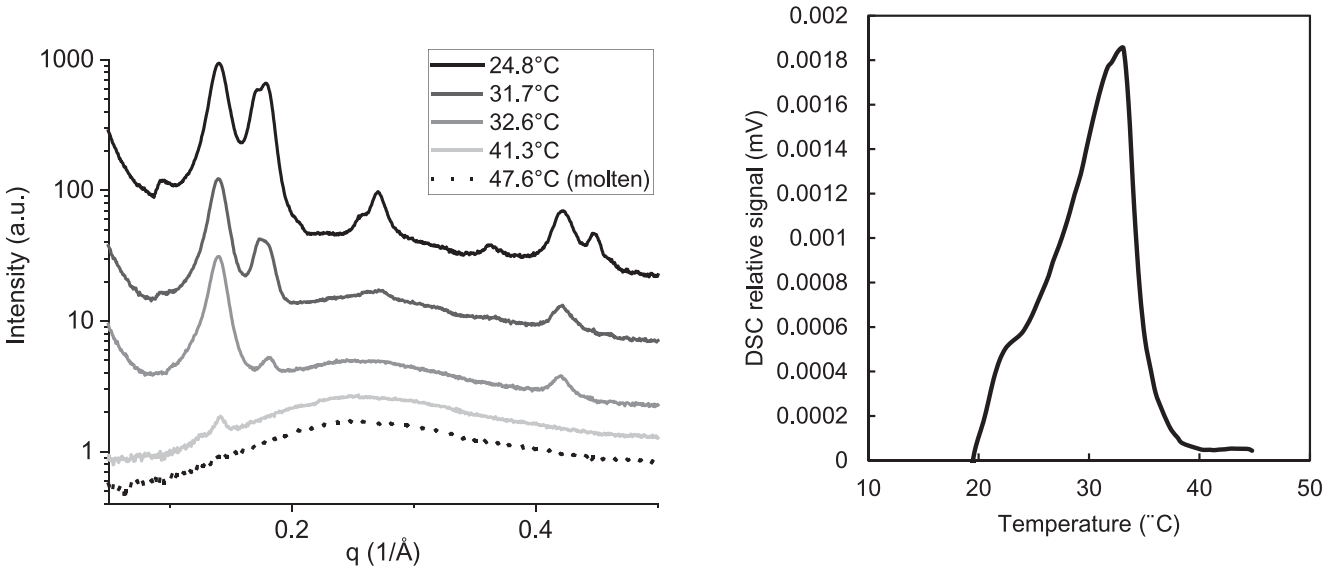

Fig. 2. DSC/SAXS data for the melting of different solid phases nucleated in samples S1. On the left the SAXS patterns at different temperatures, on the right the corresponding calorimetric signal.

The melting of α crystals and the recrystallization of the β'(2L) polymorphs are shown in the PLM measurement of Supplementary Material, Fig. S2 (no shear). The images show that the more metastable α form is detected 1 min after reaching 20 °C and keeps growing for the following 30 min; after 45 min at 20 °C these crystals start to melt at the expenses of smaller crystal agglomerates forming, the β'(2L) form.

The two SOS-rich samples (S1 and S5) showed a very different behavior compared to CB and S6. PLM experiments in the absence of shear (Supporting Information, Figs. S2 and S3) showed that S1 nucleated at higher temperature (27 °C) compared to CB (20 °C). Additionally, five different solid phases were identified during the isothermal crystallization experiments, as shown in Fig. 1c and d. The first polymorph to appear was the hexagonal α-form, with a d-spacing of 51 Å. Thereafter, still during the 120 min hold period at 20 °C, three new phases nucleated: a β'(2L) with a d-spacing of 45 Å and two 3L-structures with bigger d-spacings of 71 and around 80 Å, respectively. Most likely, these are a β'(3L) and a γ-polymorph f (Arishima et al., 1995; Mykhaylyk & Hamley, 2004). The presence of multiple distinct phases was verified by plotting the SAXS peak maximum positions (q values) as a function of their diffraction order (Miller index h; Fig. 1e and f). For lamellar phases, the peak positions fall on a straight line with slope equal to the inverse value of the d-spacing (slope = 2π/d). It is worth noting that the first order peaks for the β'(3L) and the γ-polymorph are very weak and partly obscured by the presence of the first order peak of the β-polymorph; hence, their d-spacings are mainly determined by the higher order diffraction peaks (h = 2 to 5).

Additionally, it is evident that these two 3L structures are very similar, the polymorph with larger d-spacing was labelled as the γ form based on literature data on SOS, which shows higher d-spacing for this polymorph compared to the β'(3L) (Mykhaylyk & Hamley, 2004). During the experiments, eventually, the more stable β(3L) form appeared, with a d-spacing of 65 Å. The higher d-spacings of all polymorphs of S1 and S5 compared to CB and S6 can be explained by the longer average fatty acid chain length of the first two samples compared to the latter.

After the cooling profile sample S1 was heated up to determine the melting points of the different solid phases; the results of this DSC/SAXS experiment are shown in Fig. 2.

The DSC signal from the Elettra setup is not as accurate as a conventional benchtop DSC instrument; however, it guarantees that events in DSC and SAXS perfectly line up. As shown in Supporting Information Fig. S4, the trend and onset/endpoint temperatures are consistent with

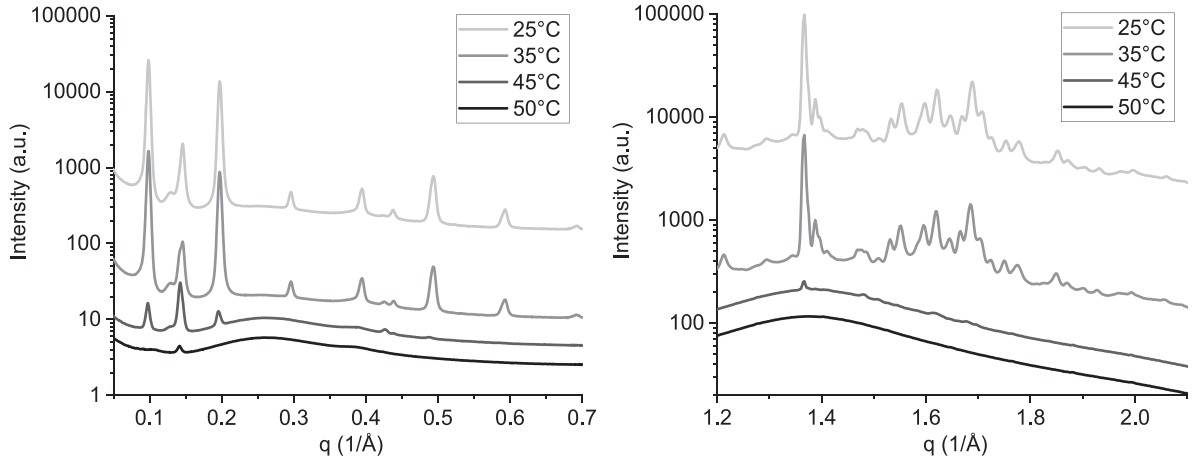

Fig. 3. Sample S1 after 6 months storage in a capillary. SAXS (left) and WAXS (right) data. The sample temperature (reported in the legend) is higher than the actual melting temperature (e.g., from DSC) as the heating rate was faster than the melting one, especially for the high melting β(2L) structures.

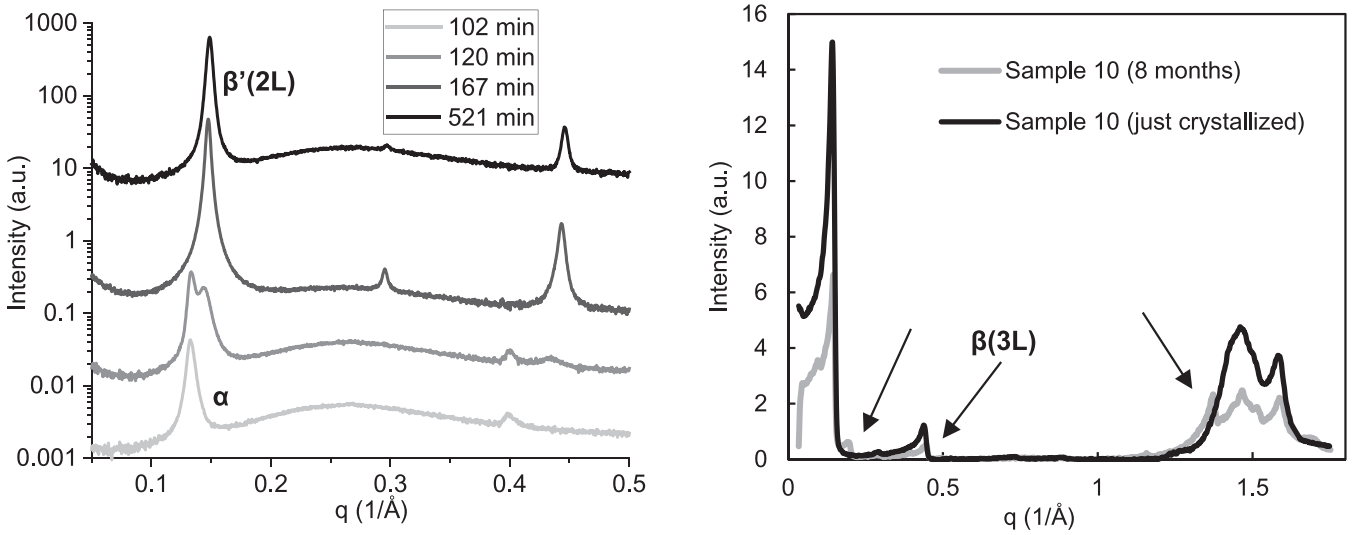

Fig. 4. sample S10 during the isothermal crystallization (left, collected at Diamond Light Source) and after several days and months after crystallization (right, collected with benchtop SAXS). Black arrows are pointing at the characteristic peaks of the β(3L) form. After six months of storage sample S10 is still a mixture of β(2L) and β'(2L) polymorphs.

the measurement carried out with a standard DSC equipment. Sample S1 is fully molten at 47.6 °C. Two different 2L polymorphs (two first order peaks still visible at 41.3 °C) persist up to around 40 °C. The more metastable β'(3L) and γ presented a melting point between 29 and 34 °C, with the β'(3L) melting slightly earlier than the γ form. The DSC trend shows a high endothermic peak between 20 and 40 °C, associated with the melting of these two metastable polymorphs as well as with the melting of the β(3L) and β'(2L) structures. Instead, a lower endothermic peak at higher temperatures is linked to the melting of the two 2L structures observed in the SAXS; these polymorphs melt later than the stable β(3L). Hence, neither of them are likely to be a β'(2L) polymorph observed nucleating after the α form.

It is worth noticing that β(2L) polymorphs do not usually appear for monosaturated TAGs such as POP, SOS and POS or their mixtures. Hence, these two polymorphs comprise of TAGs such as tri-saturated ones (SSS and PPP) or specific molecular compounds (such as stochiometric mixtures of PPO and POP or SSO and SOS), which were previously reported to form β(2L) phases (Sato & Ueno, 2005; Taguchi et al., 2021; Yao et al., 2020).

Due to the high intensity of the β'(2L) first order peak in the SAXS, it was not possible to detect the early nucleation of β(2L) phases, which are also not easily detectable in the WAXS due to their low concentration. This interpretation would explain the high melting point of these polymorphs and why they present a 2L stacking that is not commonly observed in monosaturated TAGs. A stronger proof of this hypothesis is given by the analysis of a 6 months old sample S1, shown in Fig. 3. In the SAXS region three different solid phases (one 3L and two 2L ones at q values of around 0.125 and 0.141 $Å^{-1}$) are clearly visible, with the 3L corresponding to the β(3L) polymorph observed in the cooling experiment (both SAXS and WAXS pattern are matching). Upon heating, the β(3L) polymorph melts earlier than the 2L forms, confirming that those are two different β(2L) structures originating from either tri-saturated TAGs or molecular compounds with the characteristic 2L stacking type.

Moving onto the other samples, another one that presented a very different behavior compared to CB and S6 was the POP-rich sample S10. As shown in Fig. 4 only two polymorphs nucleated during the cooling experiments, a metastable α(2L) and a β'(2L) polymorph. The morphology of the crystalline aggregate formed in this sample is shown in Supporting Information Fig. S5.

The d-spacings for both these polymorphs are smaller than the

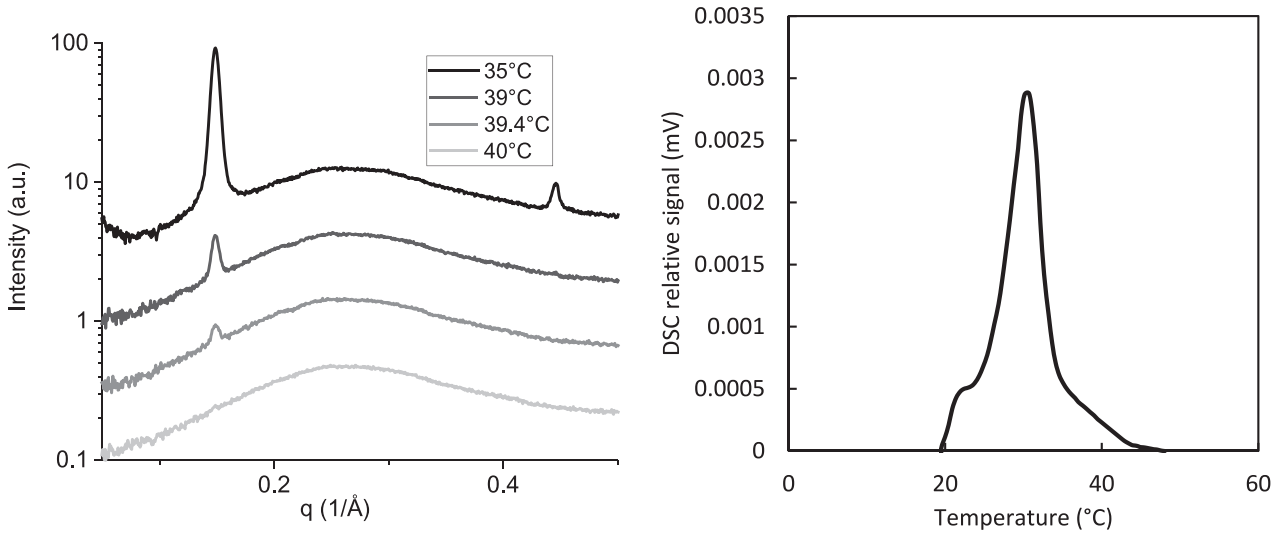

Fig. 5. DSC/SAXS data of the melting of sample S10 after the crystallization thermal profile. SAXS pattern on the left and calorimetric signal on the right.

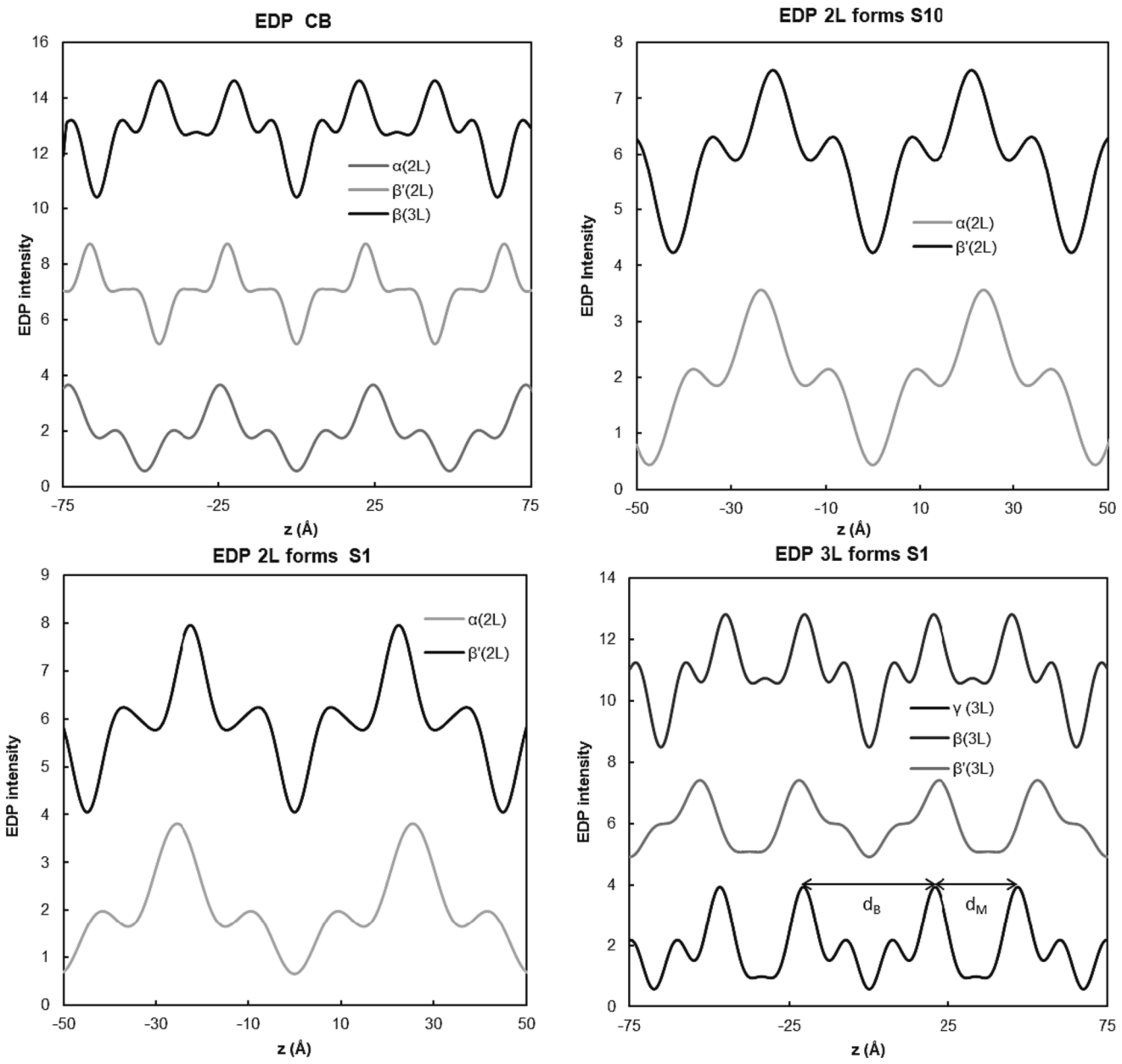

Fig. 6. Electron density profiles for the main polymorphs detected for CB, S10 and S1. The bilayer thickness, d_B, and the monolayer thickness, d_M, are defined for the 3L stacking forms.

respective ones of CB and S6 (47 and 42 Å for the α and the β' phase, respectively), due to the shorter average FA chain length of this sample. A more stable β(3L) form, with d-spacing of about 65 Å, appears after several months from the nucleation of the β'(2L); hence, the kinetics of polymorphic transformation towards this stable structure is very slow, as shown in Fig. 4b, where it is shown that after 6 months the β'(2L) polymorph still persists together with the more stable 3L structure. Despite the high amount of the relatively low melting POP (melting point of the most stable polymorph is 38 °C) and the persistence for a long time of the metastable form, sample S10 fully melts at around 40, as shown in the DSC/SAXS data of Fig. 5.

This is probably due to the high percentage of tri-saturated TAGs present in the sample. The incorporation of these molecules in the β'(2L) phase of S10 might increase the melting point for this polymorph. The high percentage (>14 %) of di- and tri-unsaturated TAGs might also explain the presence of a shoulder in the main endothermic peak during heating (which appears as two separated peaks in the standard DSC measurements, as shown in Supporting Information S6).

Fig. 6 shows the electron density profiles (EDPs) of the different polymorphs detected for CB, S1 and S10. The CB displays the well-known α(2L), β'(2L) and β(3L) stacking. Clearly, the phases condense as observed in the decaying thickness of the bilayer thickness from 49 over 44 to 42 Å. Note, for the β(3L) stacking, additionally to the bilayer thickness, d_B, the oleic-rich region, d_M is defined as $d_M = d - d_B = 22$ Å. The thinning of d_B is reflected by a zero chain-tilt in the hexagonal chain packing of the α(2L) phase, an about 28° chain tilt in the rectangular packing of the β'(2L) phase and an about 32° chain tilt in the oblique chain packing of the β'(2L) phase. Note, in our chain tilt estimations, we are assuming the glycerol backbone extension to occupy about 4 Å (Ladd Parada et al., 2018) and secondly, that the chain composition in bilayer region is practically the same for all three phases. The given 2L-phases for S10 and S1 display the same structural behavior as CB: due to the chain tilt given in the β'(2L) phase, the bilayer thickness is smaller as compared to the α(2L) phase. Interestingly, the S1 sample is the only one

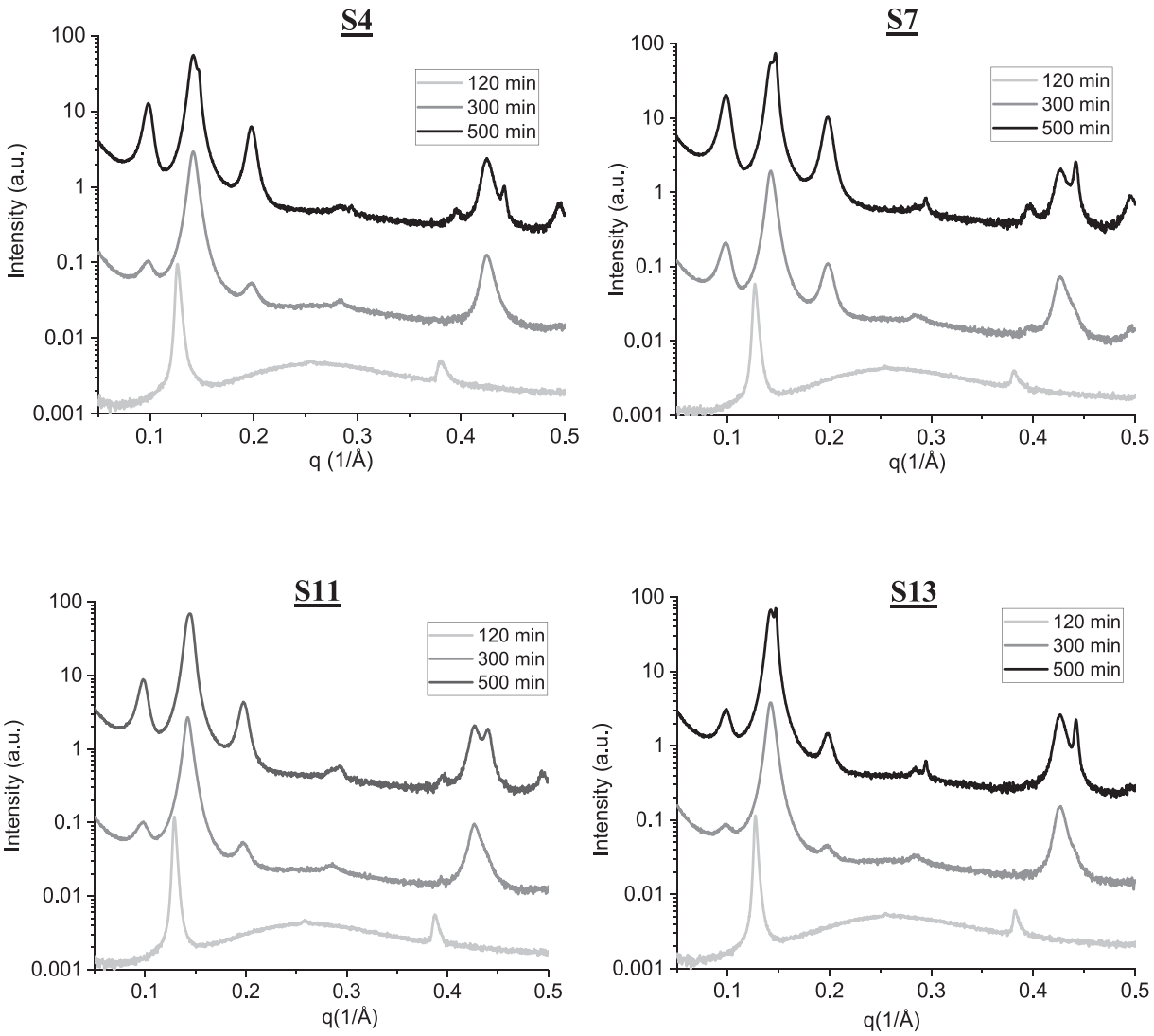

Fig. 7. SAXS pattern recorded during the crystallization experiments for samples S4, S7, S11 and S13.

displaying three different 3L-phases, namely, γ(3L), the β'(3L) and the β(3L). Again, in order of stability the bilayer thicknesses, d_B, are 45, 41 and 40 Å, respectively. While in the bilayer region mostly saturated fatty acid are apparent, the monolayer region hosts mainly the mono-unsaturated oleic acid chains. In the β(3L) the fatty acid perfectly interdigitate and display the same electron density as the CH_2 regions in the bilayer. Notably, the perfect interdigitation of chains is not realized in the monolayer regions of the β'(3L) and the γ(3L) phase. Clearly, the monounsaturated oleic acid chains are more loosely packed, since the monolayer thickness, d_M, increases from ideally 25 Å to 30 Å for the β'(3L) phase to 35 Å for the γ(3L) phase, and the electron density in the monolayer region is clearly below the CH_2 density. While this electron density increases in monolayer region from the γ(3L) to the β'(3L) and the β(3L) phase, as also observed for pure SOS (Mykhaylyk et al., 2004), the underlying molecular conformation and structures are not fully understood yet. Partially fluid oleic chains and/or traces of saturated chains in the monolayer region could both explain a relative lower chain packing density for the γ(3L) and β'(3L) phase.

Samples S2 to S4, S7 to S9 and S11 to S14 have similar amounts of SOS, POP and POS with some differences in the percentage of tri-saturated TAGs, as well as di- and tri-unsaturated TAGs. Despite the differences in chemical composition, all these samples presented a similar polymorphic behavior, as shown in Fig. 7 and Supporting Information Fig. S7. The α polymorph appeared first, followed by a β'(2L) phase with d-spacing similar to those of the SOS rich samples (S1, S5) and the two CB samples (around 44–45 Å). A β(3L) is observed within the first 500 min of experiment in all experiments apart from S8 and S14. This might be due to the lower ratio of SOS to POP contents of these two latter samples, when compared to the others. In fact, as shown earlier in samples rich in SOS (such as S1 and S5) the stable β(3L) appears within the first 250 min of the experiments; whereas for the POP-rich sample S10, this stable polymorph is not observed for several months.

For all the samples shown in Fig. 7 and Supporting Information Fig. S7, apart from S2, after about 300 min from the start of the cooling profile another solid phase with 2L stacking type appears, which is only detectable in the SAXS region and that has a d-spacing of around 43 Å. The presence of two distinct 2L phases is evident, especially when looking at their second order Bragg peaks in the region of q between 0.35 and 0.5 $Å^{-1}$, where they do not overlap as opposed to the first order ones.

The d-spacing of this latter polymorph is consistent with a 2L structure. This structure has a high melting point, above 30 °C, detected for all the samples and always melted after the stable β(3L). This behavior is consistent with the samples, where multiple β(2L) polymorphs where observed (Sato & Ueno, 2005; Taguchi et al., 2021; Yao et al., 2020). Samples S3, S7, S8, S11, S12 and S14 all contain over 1 % of tri-saturated TAGs and over 1 % of PPO, which might both form a β(2L) phase being immiscible with the more abundant β(3L). The β(2L)

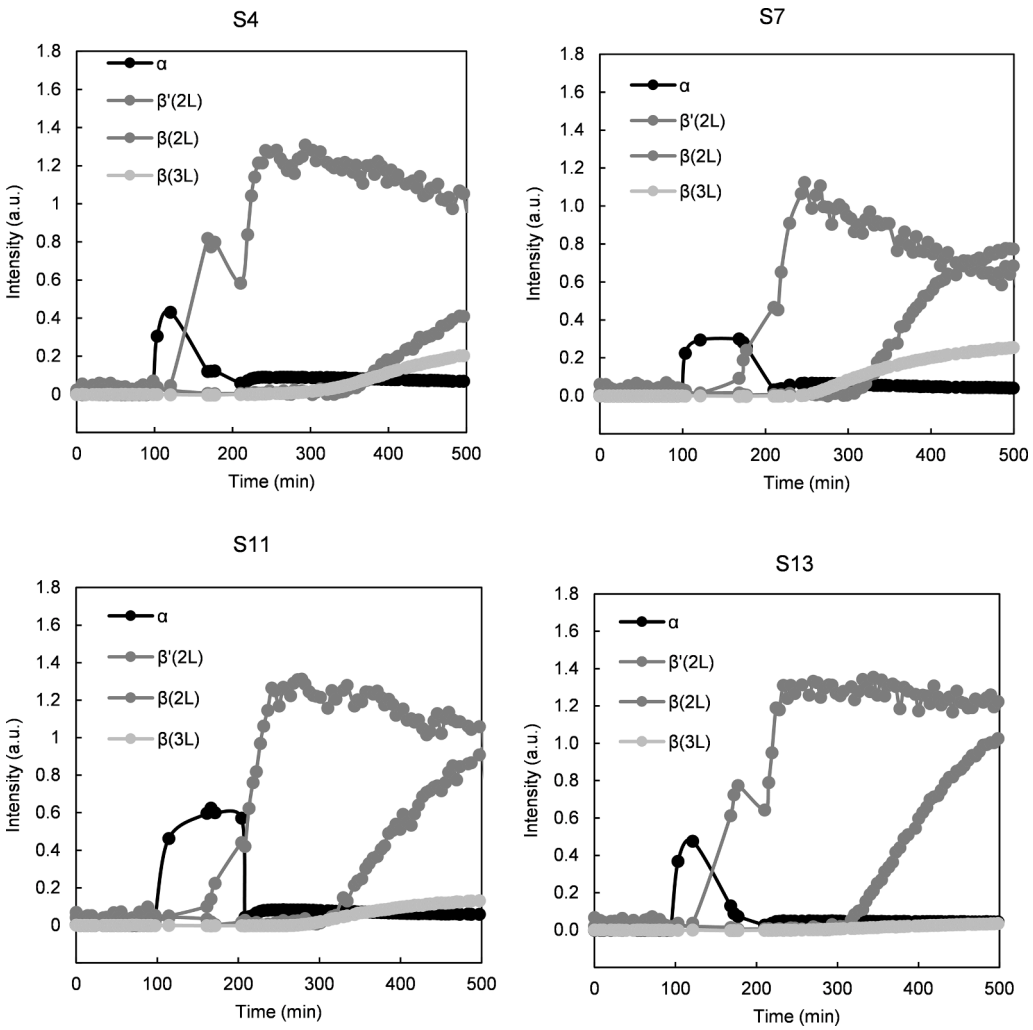

Fig. 8. Intensity of second derivative (multiplied by −1) of the pattern in correspondence with the values of the first order Bragg peak over time for samples S4, S7, S11 and S13. Evolution of the crystallization of the different polymorphs.

phase is also visible for samples containing less than 1 % of tri-saturated TAGs, particularly S4, S9 and S13. It is worth noticing, that S9 has also a low content of PPO (<1%), indicating that such a small amount of TAGs is enough to generate a visible trace of the β(2L) phase. Fig. 8 shows the intensity of the first order Bragg peak of the main phases observed in samples S4, S7, S11 and S13. It appears that the β(3L) and the β(2L) forms grow at the expense of the β'(2L), whose peaks' intensity decreases.

It is clear that a phase separation between TAGs happens as the tri-saturated β(2L) phase and the aforementioned molecular compounds of a 2L stacked phase are not miscible with β(3L) structures. A β(2L) form was not observed in 500 min long experiments for S1, S2, S5, S6 and CB. However, as previously shown even these samples displayed high melting 2L solid phases (with melting point higher than the β(3L) polymorph), when stored for over 6 months in capillaries, as shown in Fig. 9 and Supporting Information Fig. S8. The aged sample S2 presented two high melting peaks at 48 and 43 Å, similarly to S7 (47 and 43 Å), S1 (50 and 44.5 Å) and S13 (49 and 43 Å). These values are different from the d-spacings reported in literature for the β polymorphs of SSS and PPP (45 and around 41 Å, respectively; both with a melting point above 65 °C). The PPO/POP stoichiometric mixture (long spacing of 41 Å with a melting point of 31 °C), is the only molecular compound that can form considering the TAGs composition of all the CBE samples (Ghazani & Marangoni, 2023; Mishra et al., 2023). The differences in long spacing among samples might be due to the fact, that these solid phase are not pure SSS, PPP and PPO/POP but they certainly have incorporated traces of other TAGs, containing them up to their miscibility limits with these 2L structures.

For the two aged cocoa butter samples (CB and S6) three different peaks were identified in the long spacing region between 50 and 40 Å (Fig. 9), which correspond to the position of first Bragg peaks of 2L stacking type of structures (considering the average length of the FAs contained in these samples). The positions of the peaks are almost identical for CB and S6 and correspond to long spacing values of 49, 44 and 43 Å. Upon heating the last one to melt (highest melting point) was the structure with d = 44 Å. The d = 43 Å phase melted just before the β(3L), followed by the d = 49 Å crystals. While it makes great sense to identify the highest melting phase to be SSS-rich, considering its d-spacing and the high melting point (Ghazani & Marangoni, 2023), it is unclear what the other two phases correspond to. In fact, CB and S6 do not contain detectable levels of TAGs that can form molecular compounds and the melting point of PPP should be actually higher than that of the β(3L) form. Even for these two crystal types it is likely that the β(2L) polymorphs observed are TAGs mixtures including high melting SSS and PPP as well as traces over other miscible TAGs that would explain deviating melting points, when compared to pure SSS, PPP or SSS/PPP crystals.

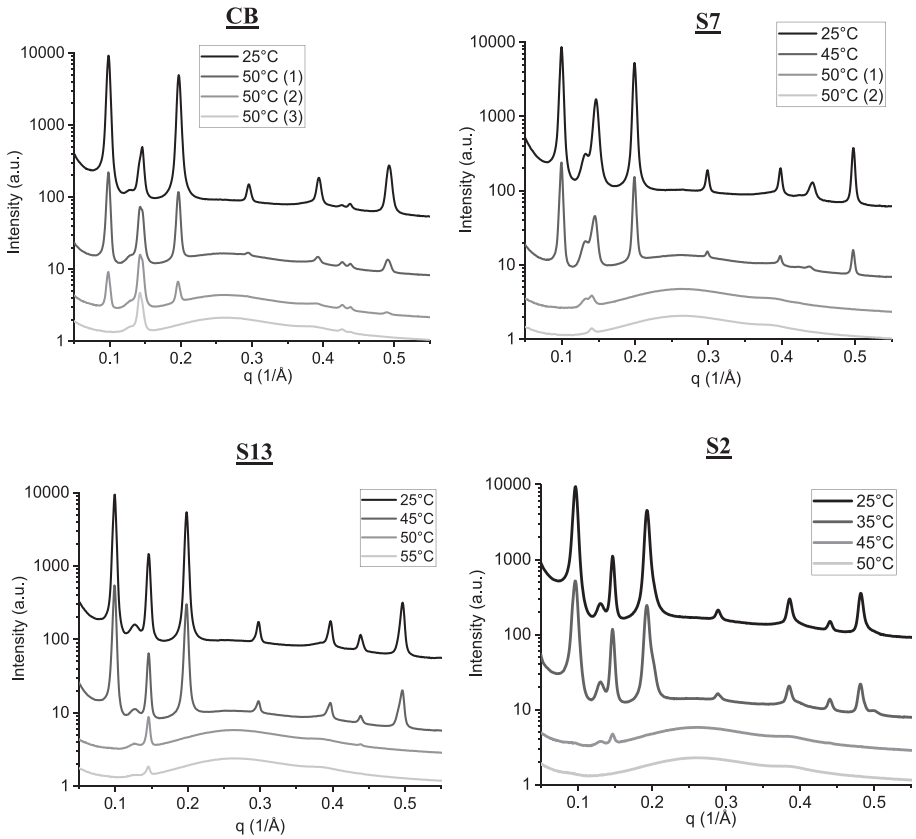

Fig. 9. Cocoa butter and CBE samples aged in capillaries after the thermal profile for over 6 months.

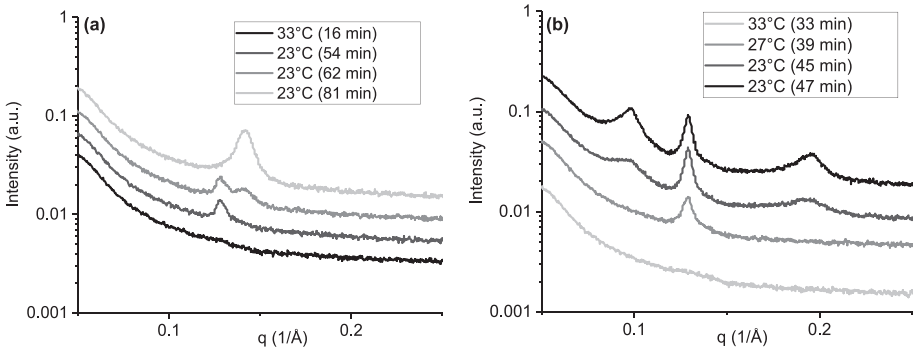

Fig. 10. (a) SAXS pattern of CB crystallized in the absence of shear at −2 °C/min from 65 °C. (b) SAXS patterns of the same samples subjected to the same temperature profile in the presence of shear (1000 s^{-1}).

3.3. Effect of shear on CBE crystallization

the effect of shear on the crystallization behavior of the CBE and CB samples was investigated with the SAXS/rheometer setup at the ESRF SAXS beamline and with PLM. It is worth noticing that, for sheared experiments, the shear was applied during the whole cooling profile. Fig. 10 and Fig. 11 show the effect of shear on sample CB. As expected based on previous literature data (MacMillan et al., 2002; Sonwai & Mackley, 2006), the presence of shear induced nucleation of cocoa butter at lower undercooling compared to the unstirred conditions (Fig. 11). Additionally, the formation of the β(3L) polymorph was observed much earlier than in the case of no shear, and this structure nucleated and grew at the expenses of the α form, without the formation of the β'(2L). This behavior is in agreement with previous literature (MacMillan et al., 2002), where shear was found to promote the formation of 3L packing structures and where a correlation between the level of shear and the rate of polymorphic transformation towards the β(3L) was observed. There are two possible reasons for this behavior; firstly, the directionality of the flow imposed by shear may force the rearrangement of TAG molecules into 3L packing types, starting from the liquid crystalline α(2L). Secondly, the shear enhanced mass transfer phenomena (convection, diffusion) might speed up polymorphic transformation into the more stable forms.

The nucleation of the two CB polymorphs is also detected in the rheometer signal (Supporting Information Fig. S9); in fact, a small increase in the viscosity value (from around 0.027 to 0.04 Pa·s) can be observed during nucleation of the α polymorph, while a larger increase (from around 0.047 to 0.2 Pa·s) was detected, when the β(3L) form appeared. Such difference might be related either to the liquid crystalline nature of the α polymorph, which might have a less significant effect on viscosity compared to the solid β(3L) polymorph, and/or to the different amount of crystals nucleated in the two events (more crystals of

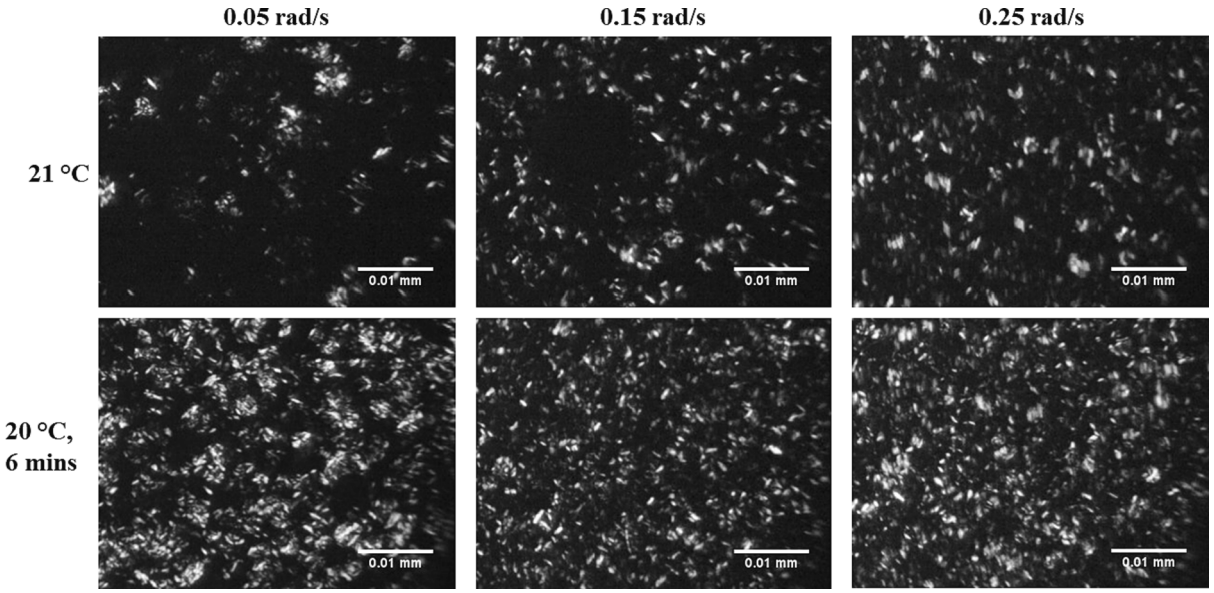

Fig. 11. CB crystallized with three levels of shear. 0.05, 0.15 and 0.25 rad/s. Images in the first row were collected at 21 °C during cooling, while those on the second row show the samples 6 min after reaching the final cooling temperature of 20 °C.

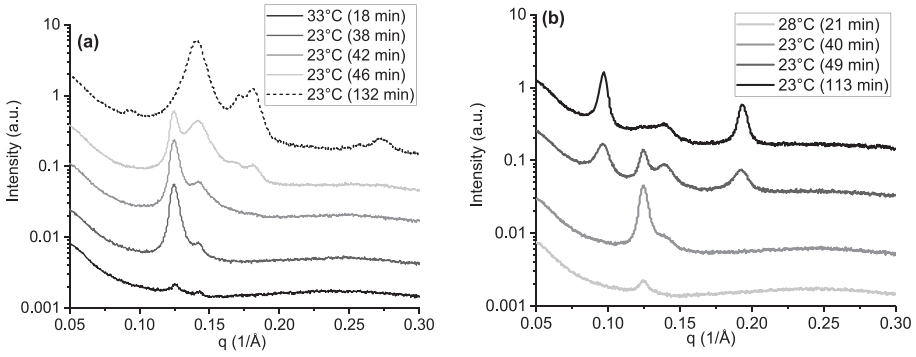

Fig. 12. (a) SAXS pattern of S1 crystallized in the absence of shear at −2°C/min from 65 °C. (b) SAXS patterns of the same samples subjected to the same temperature profile in the presence of shear (1000 s-1).

β(3L) type as compared to the α phase).

Fig. 12 and Fig. 13 show the effect of shear on sample S1, studied with SAXS and PLM. For this sample the β'(2L) polymorph was observed at around 40 min from the start of the cooling profile and the β(3L) polymorph was detected immediately after (41 min), and much earlier compared to the experiments without shearing, where this stable structure is detectable after over two hours. Remarkably, in the presence of shear the metastable β'(3L) and γ(3L) forms, which are visible after 40–42 min from the start of the cooling profile in the experiment without shearing, did not nucleate at all. Hence, even for this sample the shear promoted the formation of the β(3L) polymorph over the other more metastable structures.

Similarly to what was observed for CB, the PLM images showed an earlier nucleation point and smaller crystal agglomerates in the presence of shear (for comparison Supporting Information Fig. S3 shows the PLM images in the absence of shear for sample S1).

Crystallization experiments with shear were carried out also for samples S9 and S13 (Fig. 14), and samples S2, S7, S8 and S10 (Supporting Information Figs S10 and S11).

Samples S2 and S9 showed a behavior similar to CB, with the formation of the α polymorph and then its transformation into the β(3L), without detection of the metastable β'(2L). In sample S13, at around 50 min from the start of the cooling profile, the β'(2L) starts nucleating. The more stable β(3L) is instead detected at 65 min, and grew during the experiment at expenses of both the β'(2L) and the α polymorph. It is worth noticing a shift in the peak position of the β'(2L) polymorph from $q = 0.140$ Å^{-1} to around 0.142 Å^{-1}, which might be related to the formation of the β(2L) polymorph observed in the experiments without shearing. A similar behavior to S13 was observed in samples S7 and S8 (Supporting Information Fig. S10), with the β'(2L) appearing before the β polymorph. The additional presence of a β(2L) polymorph for sample S7 was also observed and confirmed by heating up the sample after the cooling profile. In fact, the peak at $q = 0.142$ Å^{-1} disappeared at higher temperature than the β(3L) peaks, similarly to the behavior observed in the absence of shear (shown in Supporting Information Fig. S11).

Finally, as shown in Supporting Information Fig. S10, sample S10 was the only one not showing a β(3L) polymorph during the shearing experiment. Considering the very slow kinetics of polymorphic transformation from β'(2L) to β(3L) shown in the previous sections, it is likely that the experiment was not carried out for long enough to promote the formation of the β(3L) for this CBE. Supporting Information Fig. S12 shows the PLM experiments carried out on sample 10 at different shear levels; in this case, no significant differences are observed in the morphology or amount of the crystals, when increasing the shear.

4. Conclusions

This work investigated the crystallization behavior of cocoa butter

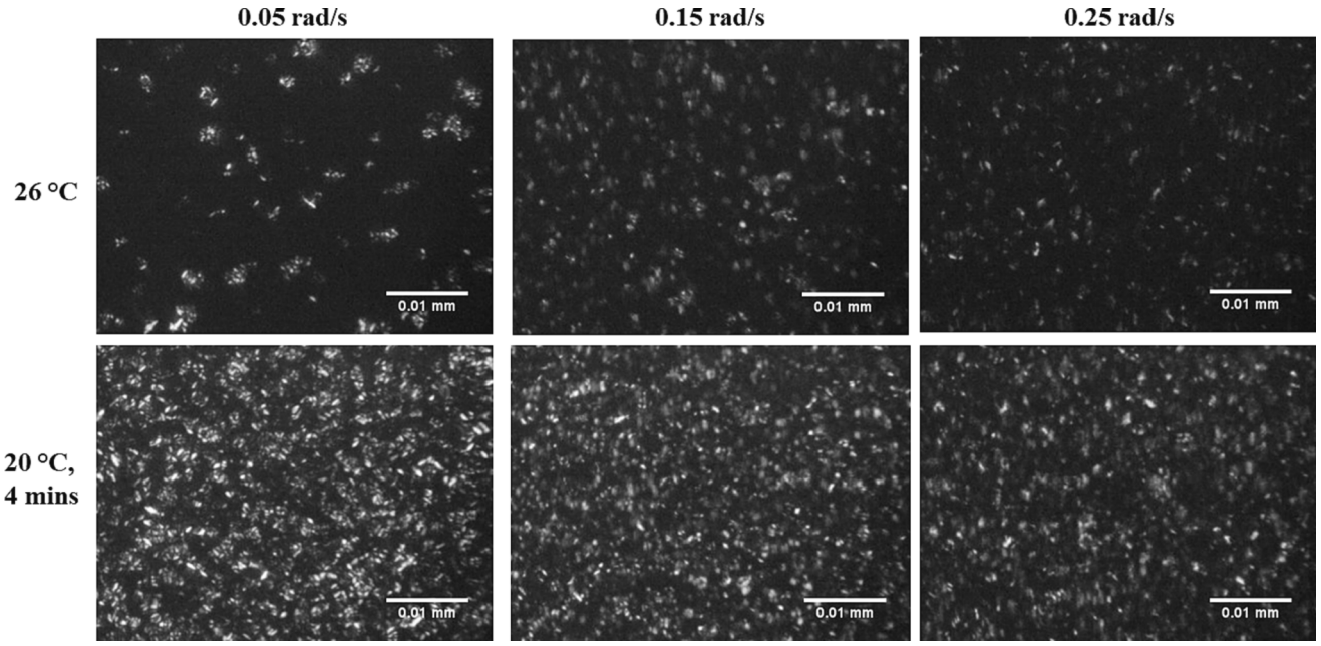

Fig. 13. S1 crystallized with three levels of shear: 0.05, 0.15 and 0.25 rad/s. Images in the first row were collected at 26 °C during cooling, while those on the second row show the samples 4 min after reaching the final cooling temperature of 20 °C.

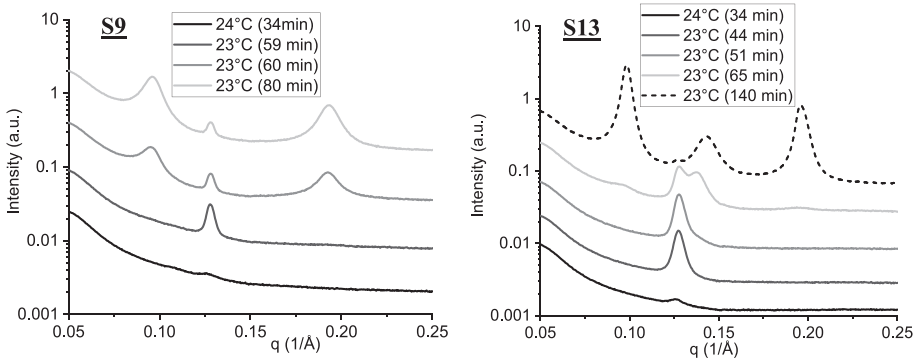

Fig. 14. Crystallization experiments with 1000 s-1 shear applied samples S9 and S13 with the SAXS/rheometer setup of beamline ID02 at ESRF.

and 13 cocoa butter equivalents of different origin. Despite some similarities in composition between CB and CBEs, these samples presented distinct crystallization behaviors. High concentration of SOS were found to form more metastable crystal structures than cocoa butter: β'(3L) and γ(3L) polymorphs were identified in the first stages of crystallization for CBEs with SOS concentration above 40 %. Whereas, the samples rich in POP presented a very slow kinetics of polymorphic transition from β'(2L) to β polymorphs (either 2 or 3L).

Tri-saturated (SSS, PPP) and pairs of TAGs forming molecular compounds (e.g., SOS/SSO, POP/PPO) were found to induce the formation of multiple stable β(2L) structures with high melting point (about 40 °C), easily detectable with SAXS even at concentrations below 1 %. The d-spacing of these polymorphs, 45 to 50 Å, is typical of a 2L type of stacking of C chains with the length of the TAGs present in CBEs. Finally, the effect of shear was investigated; shearing during cooling induced nucleation at lower level of undercooling and shear-induced secondary nucleation led to smaller crystalline aggregates at the end of the cooling profile. Shearing also had a significant effect on the polymorphs nucleated, with a significantly earlier formation of β polymorphs (both 2L and 3L) compared to the experiments without shearing and, in some cases leading to the absence of β'(2L) phase.

This work highlights the strong relationship between TAGs composition and crystallization behavior in terms of both solid form landscape and kinetics. This information is of key importance for chocolate manufacturers, who are aiming at partly replacing cocoa butter with CBEs in their formulations.

CRediT authorship contribution statement

Elena Simone: Data collection, Data curation, Formal analysis, Methodology, Writing-original draft, Writing review & editing, Conceptualization, Original idea and Funding. **Michael Rappolt:** Data curation, Formal analysis, Methodology, Writing – original draft, Writing – review & editing. **Holly Ewens:** Data curation, Formal analysis, Investigation. **Tom Rutherford:** Conceptualization, Writing – original draft. **Stephanie Marty Terrade:** Conceptualization, Writing – original draft. **Francesca Giuffrida:** Investigation. **Cynthia Marmet:** Investigation.

Declaration of competing interest

The authors declare that they have no known competing financial interests or personal relationships that could have appeared to influence the work reported in this paper.

Data availability

Data are available on Zenodo

Acknowledgment

This project received funding from the European Research Council (ERC) under the European Union's Horizon 2020 research and innovation programme (grant agreement no. 949229), and from Royal Society (grant ref. no. INF\R2\192018). We acknowledge Diamond Light Source (DLS), CERIC and ESRF for beamtime on beamlines I22, SAXS and ID02 under proposals SM26769 (DLS), 20217007, 20217066 and 20222033 (CERIC), and SC 5324 (ESRF). Finally, we are grateful to beamline scientists Prof. Nick Terrill and Dr Andrew Smith (DLS), Dr William Chevremont (ESRF), Dr Barbara Sartori and Dr Sigrid Bernstorff (CERIC, Elettra Sincrostrone Trieste) for the help and support with the three SAXS beamlines and special setups used for the work. Raw data collected on beamline ID02 at ESRF can be accessed at doi.org/10.15151/ESRF-ES-886331097.

Formatting of funding sources

Royal Society grant INF\R2\192018.

ERC Starting Grant 949229.

Diamond Light Source (UK) standard peer-reviewed access.

ESRF (France) standard peer-reviewed access.

Elettra Sincrotrone Trieste (Italy) standard CERIC peer-reviewed access.

Appendix A. Supplementary data

Supplementary data to this article can be found online at https://doi.org/10.1016/j.foodres.2023.113864.

References

Abrahamsson, S., Dahlen, B., Löfgren, H., & Pascher, I. (1978). Lateral packing of hydrocarbon chains. *Progress in the Chemistry of Fats and Other Lipids, 16*(C), 125–143. https://doi.org/10.1016/0079-6832(78)90039-3

Arishima, T., Sagi, N., Mori, H., & Sato, K. (1995). Density Measurement of the Polymorphic Forms of POP, POS and SOS. *Journal of Japan Oil Chemists' Society, 44*(6), 431–437. https://doi.org/10.5650/jos1956.44.431

Bahari, A., & Akoh, C. C. (2018). Texture, rheology and fat bloom study of 'chocolates' made from cocoa butter equivalent synthesized from illipe butter and palm mid-fraction. *Lwt, 97*(June), 349–354. https://doi.org/10.1016/j.lwt.2018.07.013

L. Bouzidi S.S. Narine Phase Behavior of Saturated Triacylglycerides-Influence of Symmetry and Chain Length Mismatch 2012 AOCS Press In Cocoa Butter and Related Compounds 10.1016/B978-0-9830791-2-5.50007-4.

Bresson, S., Lecuelle, A., Bougrioua, F., Hadri, M. E., Baeten, V., Courty, M., … Faivre, V. (2021). Comparative structural and vibrational investigations between cocoa butter (CB) and cocoa butter equivalent (CBE) by ESI / MALDI-HRMS, XRD, DSC. *MIR and Raman spectroscopy. Food Chemistry, 363*(June), Article 130319. https://doi.org/10.1016/j.foodchem.2021.130319

Burian, M., Meisenbichler, C., Naumenko, D., & Amenitsch, H. (2022). *computer programs SAXSDOG : open software for real-time azimuthal integration of 2D scattering images*. 677–685. https://doi.org/10.1107/S1600576722003685.

Campos, R., Ollivon, M., & Marangoni, A. G. (2010). *Molecular Composition Dynamics and Structure of Cocoa Butter., 10*(Lll). https://doi.org/10.1021/cg900853e

Castro-Alayo, E. M., Balcázar-Zumaeta, C. R., Torrejón-Valqui, L., Medina-Mendoza, M., Cayo-Colca, I. S., & Cárdenas-Toro, F. P. (2023). Effect of tempering and cocoa butter equivalents on crystallization kinetics, polymorphism, melting, and physical properties of dark chocolates. *Lwt, 173*(December 2022). https://doi.org/10.1016/j.lwt.2022.114402

Ewens, H., Metilli, L., & Simone, E. (2021). Analysis of the effect of recent reformulation strategies on the crystallization behaviour of cocoa butter and the structural properties of chocolate. *Current Research in Food. Science, 4*(November 2020), 105–114. https://doi.org/10.1016/j.crfs.2021.02.009

Filik, J., Ashton, A. W., Chang, P. C. Y., Chater, P. A., Day, S. J., Drakopoulos, M., … Wilhelm, H. (2017). Processing two-dimensional X-ray diffraction and small-angle scattering data in DAWN 2. *Journal of Applied Crystallography, 50*(3), 959–966. https://doi.org/10.1107/S1600576717004708

Ghazani, S. M., & Marangoni, A. G. (2019). The Ternary Solid State Phase Behavior of Triclinic POP, POS, and SOS and Its Relationship to CB and CBE Properties. *Crystal Growth and Design, 19*(2), 704–713. https://doi.org/10.1021/acs.cgd.8b01273

Ghazani, S. M., & Marangoni, A. G. (2021). Molecular Origins of Polymorphism in Cocoa Butter. *Annual Review of Food Science and Technology, 12*, 567–590. https://doi.org/10.1146/annurev-food-070620-022551

Ghazani, S. M., & Marangoni, A. G. (2023). New Triclinic Polymorph of Tristearin. *Crystal Growth & Design*. https://doi.org/10.1021/acs.cgd.2c01334

M.E. Hadri S. Bresson A. Lecuelle F. Bougrioua V. Baeten V.H. Nguyen … M. Courty applied sciences Structural and Vibrational Investigations of Mixtures of Cocoa Butter (CB), Cocoa Butter Equivalent (CBE) and Anhydrous Milk Fat (AMF) to Understand Fat Bloom Process 2022.

Ladd-Parada, M., Povey, M. J., Vieira, J., & Ries, M. E. (2019). Fast field cycling NMR relaxometry studies of molten and cooled cocoa butter. *Molecular Physics, 117*(7–8), 1020–1027. https://doi.org/10.1080/00268976.2018.1508784

Ladd Parada, M., Sadeghpour, A., Vieira, J., Povey, M., & Rappolt, M. (2018). Global Small-Angle X-ray Scattering Data Analysis of Triacylglycerols in the α-Phase (Part II). *Journal of Physical Chemistry B, 122*(45), 10330–10336. https://doi.org/10.1021/acs.jpcb.8b06708

Lipp, M., Simoneau, C., Ulberth, F., Anklam, E., Crews, C., Brereton, P., … Wiedmaier, C. (2001). Composition of genuine cocoa butter and cocoa butter equivalents. *Journal of Food Composition and Analysis, 14*(4), 399–408. https://doi.org/10.1006/jfca.2000.0984

MacMillan, S. D., Roberts, K. J., Rossi, A., Wells, M. A., Polgreen, M. C., & Smith, I. H. (2002). In situ small angle X-ray Scattering (SAXS) studies of polymorphism with the associated crystallization of cocoa butter fat using shearing conditions. *Crystal Growth and Design, 2*(3), 221–226. https://doi.org/10.1021/cg0155649

Marty-Terrade, S., & Marangoni, A. G. (2012). Impact of cocoa butter origin on crystal behavior. *Cocoa Butter and Related Compounds, 245–274*. https://doi.org/10.1016/B978-0-9830791-2-5.50014-1

Metilli, L., Lazidis, A., Francis, M., Marty-Terrade, S., Ray, J., & Simone, E. (2021). The effect of crystallization conditions on the structural properties of oleofoams made of cocoa butter crystals and high oleic sunflower oil. *Crystal Growth and Design, 21*(3), 1562–1575. https://doi.org/10.1021/acs.cgd.0c01361

Metilli, L., Storm, M., Marathe, S., Lazidis, A., Marty-Terrade, S., & Simone, E. (2022). Application of X-ray Microcomputed Tomography for the Static and Dynamic Characterization of the Microstructure of Oleofoams. *Langmuir, 38*(4), 1638–1650. https://doi.org/10.1021/acs.langmuir.1c03318

Mishra, K., Kummer, N., Bergfreund, J., Kämpf, F., Bertsch, P., Pauer, R., … Windhab, E. J. (2023). Controlling lipid crystallization across multiple length scales by directed shear flow. *Journal of Colloid and Interface Science, 630*, 731–741. https://doi.org/10.1016/j.jcis.2022.10.005

Mykhaylyk, O. O., Castelletto, V., Hamley, I. W., & Povey, M. J. W. (2004). Structure and transformation of low-temperature phases of 1,3-distearoyl-2-oleoyl glycerol. *European Journal of Lipid Science and Technology, 106*(5), 319–324. https://doi.org/10.1002/ejlt.200300926

Mykhaylyk, O. O., & Hamley, I. W. (2004). The packing of triacylglycerols from SAXS measurements: Application to the structure of 1,3-distearoyl-2-oleoyl-sn-glycerol crystal phases. *Journal of Physical Chemistry B, 108*(23), 8069–8083. https://doi.org/10.1021/jp0379704

Nagy, K., Sandoz, L., Destaillats, F., & Schafer, O. (2013). Mapping the regioisomeric distribution of fatty acids in triacylglycerols by hybrid mass spectrometry. *Journal of Lipid Research, 54*. https://doi.org/10.1194/jlr.D031484

Narayanan, T., Sztucki, M., Vaerenbergh, P. Van, Gorini, J., Claustre, L., Sever, F., & Morse, J. (2018). *A multipurpose instrument for time-resolved ultra- small-angle and coherent X-ray scattering research papers*. 1511–1524. https://doi.org/10.1107/S1600576718012748.

Norazlina, M. R., Jahurul, M. H. A., Hasmadi, M., Mansoor, A. H., Norliza, J., Patricia, M., … Fan, H. Y. (2021). Trends in blending vegetable fats and oils for cocoa butter alternative application: A review. *Trends in Food Science and Technology, 116*(March), 102–114. https://doi.org/10.1016/j.tifs.2021.07.016

Ollivon, M., Keller, G., Bourgaux, C., Kalnin, D., Villeneuve, P., & Lesieur, P. (2006). DSC and high resolution X-ray diffraction coupling. *Journal of Thermal Analysis and Calorimetry, 85*(1), 219–224. https://doi.org/10.1007/s10973-005-7351-y

Pirouzian, H. R., Konar, N., Palabiyik, I., Oba, S., & Toker, O. S. (2020). Pre-crystallization process in chocolate: Mechanism, importance and novel aspects. *Food Chemistry, 321*(March), Article 126718. https://doi.org/10.1016/j.foodchem.2020.126718

Pratama, Y., Burholt, S., Baker, D. L., Sadeghpour, A., Simone, E., & Rappolt, M. (2022). Polymorphism of a Highly Asymmetrical Triacylglycerol in Milk Fat: 1-Butyryl 2-Stearoyl 3-Palmitoyl-glycerol. *Crystal Growth and Design, 22*(10), 6120–6130. https://doi.org/10.1021/acs.cgd.2c00713

Ramos-de-la-Peña, A. M., Aguilar, O., & González-Valdez, J. (2021). Progress in nanostructure understanding of edible crystalline fats and their application in nano-delivery systems: Cocoa butter as a model. *Food Research International, 147*(December 2020). https://doi.org/10.1016/j.foodres.2021.110561

Rappolt, M., Laggner, P., & Pabst, G. (2004). Structure and elasticity of phospholipid bilayers in the La phase: A comparison of phosphatidylcholine and phosphatidylethanolamine membranes. In *Recent Research Developments in Biophysics* (pp. 365–394). Trivandrum: Transworld Research Network.

Sasaki, M., Ueno, S., & Sato, K. (2012). Polymorphism and mixing phase behavior of major triacylglycerols of cocoa butter. *Cocoa Butter and Related Compounds, 151–172*. https://doi.org/10.1016/B978-0-9830791-2-5.50009-8

Sato, K., & Ueno, S. (2005). Polymorphism in Fats and Oils. *Bailey's Industrial Oil and Fat Products, 77–120*. https://doi.org/10.1002/047167849x.bio020

Sivakanthan, S., & Madhujith, T. (2020). Current trends in applications of enzymatic interesterification of fats and oils: A review. *Lwt, 132*(July), Article 109880. https://doi.org/10.1016/j.lwt.2020.109880

Small, D. M. (1984). Lateral chain packing in lipids and membranes. *Journal of Lipid Research, 25*(13), 1490–1500. https://doi.org/10.1016/s0022-2275(20)34422-9

Sonwai, S., & Mackley, M. R. (2006). The effect of shear on the crystallization of cocoa butter. *JAOCS, Journal of the American Oil Chemists' Society, 83*(7), 583–596. https://doi.org/10.1007/s11746-006-1243-6

Taguchi, K., Toda, A., Hondoh, H., Ueno, S., & Sato, K. (2021). Kinetic study on alpha-form crystallization of mixed-acid triacylglycerols POP, PPO, and Their Mixture. *Molecules, 26*(1), 1–13. https://doi.org/10.3390/MOLECULES26010220

Timms, R. E. (1984). Phase behaviour of fats and their mixtures. *Progress in Lipid Research, 23*(1), 1–38. https://doi.org/10.1016/0163-7827(84)90004-3

Toro-Vazquez, J. F., Charó-Alonso, M. A., Morales-Rueda, J. A., & Pérez-Martínez, J. D. (2012). Molecular Interactions of Triacylglycerides in Blends of Cocoa Butter with trans-free Vegetable Oils. *Cocoa Butter and Related Compounds, 393–416*. https://doi.org/10.1016/B978-0-9830791-2-5.50019-0

Yao, Y., Liu, W., Zhang, D., Li, R., Zhou, H., Li, C., & Wang, S. (2020). Dynamic changes in the triacylglycerol composition and crystallization behavior of cocoa butter. *Lwt, 129*(March), Article 109490. https://doi.org/10.1016/j.lwt.2020.109490